Micromorphic continuum. Part III: Small deformation plasticity coupled with damage

P. Grammenoudis, Ch. Tsakmakis, D. Hofer

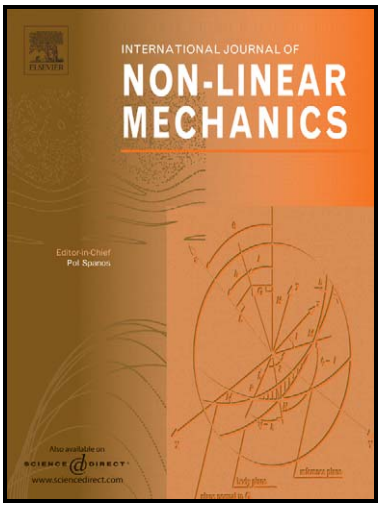

www.elsevier.com/locate/nlm

Micromorphic continuum. Part III: Small deformation plasticity coupled with damage

P. Grammenoudis, Ch. Tsakmakis, D. Hofer

PII: S0020-7462(09)00184-X
DOI: doi:10.1016/j.ijnonlinmec.2009.10.003
Reference: NLM 1654

To appear in: *International Journal of Non-Linear Mechanics*

Received date: 7 July 2008
Revised date: 12 October 2009
Accepted date: 13 October 2009

Cite this article as: P. Grammenoudis, Ch. Tsakmakis and D. Hofer, Micromorphic continuum. Part III: Small deformation plasticity coupled with damage, *International Journal of Non-Linear Mechanics*, doi:10.1016/j.ijnonlinmec.2009.10.003

Micromorphic continuum. Part III: Small deformation plasticity coupled with damage

P. Grammenoudis * and Ch. Tsakmakis **

Darmstadt University of Technology

Institute of Continuum Mechanics

Hochschulstraße 1, D-64289 Darmstadt, Germany

D. Hofer

Westinghouse Electric Germany GmbH

Abt. PEM, Dudenstr. 44, D-68167 Mannheim, Germany

Abstract

Properties of the micromorphic theory proposed in Part II are discussed for the case of small deformations. Model responses for beam specimens under bending loading and plates with circular holes under tension loading are calculated by employing the finite element method. The results reported are concerned with the capabilities of the theory to predict size effects.

Key words: micromorphic plasticity; finite deformation; isotropic and kinematic hardening rules; isotropic continuum damage mechanics; finite element implementation;

Preprint submitted to International Journal of Non-Linear Mechanics19 August 2009

1 Introduction

A finite deformation micromorphic plasticity theory, exhibiting isotropic and kinematic hardening, and incorporating damage effects, has been proposed in Part II. The theory is consistent with the second law of thermodynamics and deals with a plastic micromorphic curvature tensor, which is not required to fulfill some compatibility conditions, i.e. it is not related to some gradient terms. Furthermore, a measure of smallness ε has been introduced in Part II, and the theory has been defined to be of small deformations, if terms only up to order $O(\varepsilon)$ are retained. It is a straightforward task to verify that the small deformation version of the micromorphic model proposed, reads as follows (we confine attention to static balance equations and omit the body and double body forces).

Equilibrium equations

$$\frac{\partial T_{ij}}{\partial X_j} = 0 \quad \text{in } \mathcal{R}_{\mathcal{R}} \quad , \tag{1}$$

$$\frac{\partial \mathcal{T}_{ijk}}{\partial X_k} + T_{ij} - \Sigma_{ij} = 0 \quad \text{in } \mathcal{R}_{\mathcal{R}} \quad . \tag{2}$$

Boundary conditions

$$T_{ij} n_j = \bar{t}_i \quad \text{on } \partial\mathcal{R}_{\mathcal{R}}^{t_i} = \partial\mathcal{R}_{\mathcal{R}} \setminus \partial\mathcal{R}_{\mathcal{R}}^{u_i} \quad , \tag{3}$$

$$\mathcal{T}_{ijk} n_k = \bar{t}_{ij}^{(d)} \quad \text{on } \partial\mathcal{R}_{\mathcal{R}}^{t_{ij}^{(d)}} = \partial\mathcal{R}_{\mathcal{R}} \setminus \partial\mathcal{R}_{\mathcal{R}}^{h_{ij}} \quad , \tag{4}$$

$$u_i = \bar{u}_i \quad \text{on } \partial\mathcal{R}_{\mathcal{R}}^{u_i} \quad , \tag{5}$$

* Corresponding author.
**Corresponding author.
Email addresses: pascha@mechanik.tu-darmstadt.de (P. Grammenoudis), tsakmakis@mechanik.tu-darmstadt.de (Ch. Tsakmakis).

$$h_{ij} = \bar{h}_{ij} \quad \text{on } \partial\mathcal{R}_{\mathcal{R}}^{h_{ij}} \quad . \tag{6}$$

Kinematics

$$H_{ij} = \frac{\partial u_i}{\partial X_j} \quad , \tag{7}$$

$$\beta_{ij} = \frac{1}{2}(h_{ij} + h_{ji}) \quad , \quad \epsilon_{ij} = H_{ij} - h_{ij} \quad , \quad \mathcal{K}_{ijk} = \frac{\partial h_{ij}}{\partial X_k} \quad , \tag{8}$$

$$\beta_{ij} = (\boldsymbol{\beta}_e)_{ij} + (\boldsymbol{\beta}_p)_{ij} \quad , \quad \epsilon_{ij} = (\boldsymbol{\epsilon}_e)_{ij} + (\boldsymbol{\epsilon}_p)_{ij} \quad , \quad \mathcal{K}_{ijk} = (\boldsymbol{\mathcal{K}}_e)_{ijk} + (\boldsymbol{\mathcal{K}}_p)_{ijk} \quad . \tag{9}$$

Specific free energy

$$\Psi = \Psi_e + \Psi_{is} + \Psi_k \quad . \tag{10}$$

Elasticity laws

$$\begin{aligned} \varrho\Psi_e =& (1-D)\left\{\frac{1}{2}(\mathbb{A}_e)_{ijpq}(\boldsymbol{\epsilon}_e)_{ij}(\boldsymbol{\epsilon}_e)_{pq} + \frac{1}{2}(\mathbb{B}_e)_{ijpq}(\boldsymbol{\beta}_e)_{ij}(\boldsymbol{\beta}_e)_{pq}\right. \\ &\left. +(\mathbb{D}_e)_{ijpq}(\boldsymbol{\epsilon}_e)_{ij}(\boldsymbol{\beta}_e)_{pq} + \frac{1}{2}(\boldsymbol{\mathcal{C}}_e)_{ijpqr}(\boldsymbol{\mathcal{K}}_e)_{ijk}(\boldsymbol{\mathcal{K}}_e)_{pqr}\right\} \quad , \end{aligned} \tag{11}$$

$$\Sigma_{ij} = \varrho\frac{\partial\Psi_e}{\partial(\boldsymbol{\beta}_e)_{ij}} = (1-D)\{(\mathbb{B}_e)_{ijpq}(\boldsymbol{\beta}_e)_{pq} + (\mathbb{D}_e)_{ijpq}(\boldsymbol{\epsilon}_e)_{pq}\} \quad , \tag{12}$$

$$T_{ij} = \varrho\frac{\partial\Psi_e}{\partial(\boldsymbol{\epsilon}_e)_{ij}} = (1-D)\{(\mathbb{A}_e)_{ijpq}(\boldsymbol{\epsilon}_e)_{pq} + (\mathbb{D}_e)_{ijpq}(\boldsymbol{\beta}_e)_{pq}\} \quad , \tag{13}$$

$$\mathcal{T}_{ijk} = \varrho\frac{\partial\Psi_e}{\partial(\boldsymbol{\mathcal{K}}_e)_{ijk}} = (1-D)(\boldsymbol{\mathcal{C}}_e)_{ijkpqr}(\boldsymbol{\mathcal{K}}_e)_{pqr} \quad . \tag{14}$$

Yield function

$$\begin{aligned} f =& \frac{1}{1-D}\left((T_{ij}-T_{ij}^k)^D(\mathbb{A}_y)_{ijpq}(T_{pq}-T_{pq}^k)^D + (\Sigma_{ij}-\Sigma_{ij}^k)^D(\mathbb{B}_y)_{ijpq}(\Sigma_{pq}-\Sigma_{pq}^k)^D\right. \\ &\left. +(\mathcal{T}_{ijk}-\mathcal{T}_{ijk}^k)^D(\boldsymbol{\mathcal{C}}_y)_{ijkpqr}(\mathcal{T}_{pqr}-\mathcal{T}_{pqr}^k)^D\right)^{-\frac{1}{2}} - \frac{R}{1-D} - \bar{k}_0 \quad , \end{aligned} \tag{15}$$

$$k := \frac{R}{1-D} + \bar{k}_0 \quad , \quad k := R_0 + \bar{k}_0 \quad . \tag{16}$$

Flow rule

$$(\dot{\boldsymbol{\epsilon}}_p)_{ij} = \frac{\dot{s}}{\zeta}\frac{\partial f}{\partial T_{ij}} \quad , \quad (\dot{\boldsymbol{\beta}}_p)_{ij} = \frac{\dot{s}}{\zeta}\frac{\partial f}{\partial \Sigma_{ij}} \quad , \quad (\dot{\boldsymbol{\mathcal{K}}}_p)_{ijk} = \frac{\dot{s}}{\zeta}\frac{\partial f}{\partial \mathcal{T}_{ijk}} \quad , \tag{17}$$

$$\zeta := \sqrt{\frac{\partial f}{\partial T_{ij}}\frac{\partial f}{\partial T_{ij}} + \frac{\partial f}{\partial \Sigma_{ij}}\frac{\partial f}{\partial \Sigma_{ij}} + \frac{\partial f}{\partial \mathcal{T}_{ijk}}\frac{\partial f}{\partial \mathcal{T}_{ijk}}} \quad . \tag{18}$$

Plasticity

$$L(t) := [\dot{f}(t)]_{s=\text{const.}} \tag{19}$$

$$\dot{s} \begin{cases} > 0 \text{ for } f = 0 \ \& \ L > 0 \quad , \\ = 0 \text{ otherwise} \quad , \end{cases} \tag{20}$$

$$\dot{s} \quad : \quad \text{to be determined from consistency condition } \dot{f} = 0 \quad . \tag{21}$$

Viscoplasticity

$$\dot{s} := \frac{\langle f \rangle^m}{\eta} \geq 0 \quad , \tag{22}$$

$$\langle f \rangle \quad : \quad \text{overstress} \quad . \tag{23}$$

Isotropic hardening

$$\varrho\Psi_{is} = (1-D)\frac{\gamma}{2}(r^2 + 2r_0 r) \quad , \tag{24}$$

$$R = \varrho\frac{\partial \Psi_{is}}{\partial r} = (1-D)\gamma(r + r_0) = (1-D)(\gamma r + R_0) \quad , \tag{25}$$

$$\dot{r} = (1 - \beta r)\frac{\dot{s}}{\zeta} \quad . \tag{26}$$

Kinematic hardening

$$\begin{aligned} \varrho\Psi_k =& (1-D)\left\{\frac{1}{2}(\mathbb{A}_k)_{ijpq}(\boldsymbol{\epsilon}_k)_{ij}(\boldsymbol{\epsilon}_k)_{pq} + \frac{1}{2}(\mathbb{B}_k)_{ijpq}(\boldsymbol{\beta}_k)_{ij}(\boldsymbol{\beta}_k)_{pq}\right. \\ &\left. + (\mathbb{D}_k)_{ijpq}(\boldsymbol{\epsilon}_k)_{ij}(\boldsymbol{\beta}_k)_{pq} + \frac{1}{2}(\boldsymbol{\mathcal{C}}_k)_{ijpqr}(\boldsymbol{\mathcal{K}}_k)_{ijk}(\boldsymbol{\mathcal{K}}_k)_{pqr}\right\} \quad , \end{aligned} \tag{27}$$

$$(\boldsymbol{\Sigma}_k)_{ij} = \varrho \frac{\partial \Psi_k}{\partial (\boldsymbol{\beta}_k)_{ij}} = (1-D)\{(\mathbb{B}_k)_{ijpq}(\boldsymbol{\beta}_k)_{pq} + (\mathbb{D}_k)_{ijpq}(\boldsymbol{\epsilon}_k)_{pq}\} \quad , \tag{28}$$

$$(\mathbf{T}_k)_{ij} = \varrho \frac{\partial \Psi_k}{\partial (\boldsymbol{\epsilon}_k)_{ij}} = (1-D)\{(\mathbb{A}_k)_{ijpq}(\boldsymbol{\epsilon}_k)_{pq} + (\mathbb{D}_k)_{ijpq}(\boldsymbol{\beta}_k)_{pq}\} \quad , \tag{29}$$

$$(\boldsymbol{\mathcal{T}}_k)_{ijk} = \varrho \frac{\partial \Psi_k}{\partial (\boldsymbol{\mathcal{K}}_k)_{ijk}} = (1-D)(\boldsymbol{\mathcal{C}}_k)_{ijkpqr}(\boldsymbol{\mathcal{K}}_k)_{pqr} \quad , \tag{30}$$

$$\dot{\boldsymbol{\epsilon}}_k = \dot{\boldsymbol{\epsilon}}_p - \frac{\dot{s}}{1-D}\{M_1^k(\mathrm{tr}\mathbf{T}_k)\mathbf{1} + M_2^k\mathbf{T}_k + M_3^k(\mathbf{T}_k)^T\} \quad , \tag{31}$$

$$\dot{\boldsymbol{\beta}}_k = \dot{\boldsymbol{\beta}}_p - \frac{\dot{s}}{1-D}\{N_1^k(\mathrm{tr}\boldsymbol{\Sigma}_k)\mathbf{1} + 2N_2^k\boldsymbol{\Sigma}_k\} \quad , \tag{32}$$

$$\dot{\boldsymbol{\mathcal{K}}}_k = \dot{\boldsymbol{\mathcal{K}}}_p - \frac{\dot{s}}{1-D}\hat{\boldsymbol{\mathcal{P}}}_k[\boldsymbol{\mathcal{T}}] \quad . \tag{33}$$

Evolution law for damage

$$\dot{D} = -\alpha_1 \dot{s} \varrho \frac{\partial \Psi}{\partial D} \quad . \tag{34}$$

The aim of the present paper is to demonstrate the capabilities of this model in describing size effects present in bending of beam specimens and in plates with a hole under tension loading. It should be remarked that Part I and II made it clear, that micromorphic constitutive theories are very complex and include a large number of material parameters. Therefore, we decided to make transparent capabilities of such theories only for small deformations, excluding from considerations geometrical nonlinearities. Also, several material parameters will be assumed to vanish, in order to reduce the effort of the analysis. Of course, this implies that important capabilities of the model may be not activated. However, the present investigation is not entitled to be complete and will be of qualitative character only. This also concerns the isotropic hardening rule. In fact, isotropic hardening effects due to strains and micromorphic curvature tensors are captured in a unified manner. There are, however, possibilities to account for isotropic hardening effects due to strain and micromorphic curvature effects separately. Such isotropic hardening rules

have been elaborated by Grammenoudis and Tsakmakis (2008) in micropolar plasticity and are not pursuit here.

2 Examples

Examples illustrating the capabilities of the theory to capture size effects are given in this section and are taken from the doctoral thesis of Hofer (2003), where also more details about the implementation are given. Further examples and interesting results on this topic may be found in Dillard and Ienny (2006); Kirchner and Steinmann (2005); Neff and Forest (2007); Lazar and Maugin (2007) as well as Hirschberger and Steinmann (2007).

In the ensuing analysis, the chosen values of the material parameters do not reflect some responses of realistic material behavior, i.e., they are only of academic interest and serve to discuss basic features of the model. We set

$$A_1^e \equiv \lambda = 1,21 \cdot 10^5 N/mm^2 \quad , \quad A_2^e = \mu + \alpha \quad , \quad A_3^e = \mu - \alpha \quad , \tag{35}$$

$$\mu = 8,08 \cdot 10^4 N/mm^2 \quad , \tag{36}$$

$$B_1^e \equiv \lambda \quad , \quad B_2^e \equiv \mu + b_2 \quad , \quad b_2 = 10 \cdot \mu \quad , \tag{37}$$

$$D_1^e \equiv \lambda \quad , \quad D_2^e \equiv \mu \quad , \tag{38}$$

$$C_i^e = 0 \quad \text{for } i \neq 7 \quad , \quad C_7^e = c_7 \geq 0 \quad . \tag{39}$$

Although for the case (39), important aspects of the constitutive model may be retain inactive, we shall confine ourself on this special case in order to limit the discussion. For what follows, of particular interest is the internal length

$$l_c := \sqrt{\frac{c_7}{\mu}} \quad , \tag{40}$$

suggested by the elasticity laws. Firstly, we shall discuss micromorphic elasticity without damage (pure micromorphic elasticity).

2.1 Pure micromorphic elasticity

2.1.1 Rectangular specimens with circular hole under tension loading

Consider the plane strain problem in Fig. 1 where the quadratic section (length b) with a circular hole (radius r) located in the center of the section, is stretched in y direction. With respect to the Cartesian coordinate system x, y, the boundaries $x = \pm\frac{b}{2}$ are assumed to be traction-free. At the boundary $y = -\frac{b}{2}$ the displacement u_y and the traction t_x are assumed to vanish, while at the boundary $y = \frac{b}{2}$, given displacement u_y and traction $t_x = 0$ are imposed. The whole circular hole is assumed to be traction free, while the whole boundary is subjected to vanishing double traction $\mathbf{t}^{(d)}$.

For small circular hole, a nearly uniform stress component σ_0 in y direction, at $y = \frac{b}{2}$, will be required to realize the given boundary conditions. In classical elasticity, attention is focussed on the so-called stress concentration factor

$$\frac{T^{\star}_{yy}}{\sigma_0} \quad , \quad T^{\star}_{yy} := T_{yy}(x = r, y = 0) \quad , \tag{41}$$

which turns out to be equal to 3 (see e.g. Gould, 1983, p. 124), whenever the section is of infinite extension b. In the present context, we refer to as classical, the case where $\alpha \approx 0$, $c_7 \approx 0$, which are approximated numerically for given values of b, r. Particularly, we set $b = 2,5mm$ and $r = 0,25mm$, which imply the value $\frac{T^{\star}_{yy}}{\sigma_0} = 3,14$. Typical properties of micromorphic elasticity may be elucidated by regarding the distribution of $\frac{T_{yy}}{\sigma_0}$ along the line $y = 0$ and

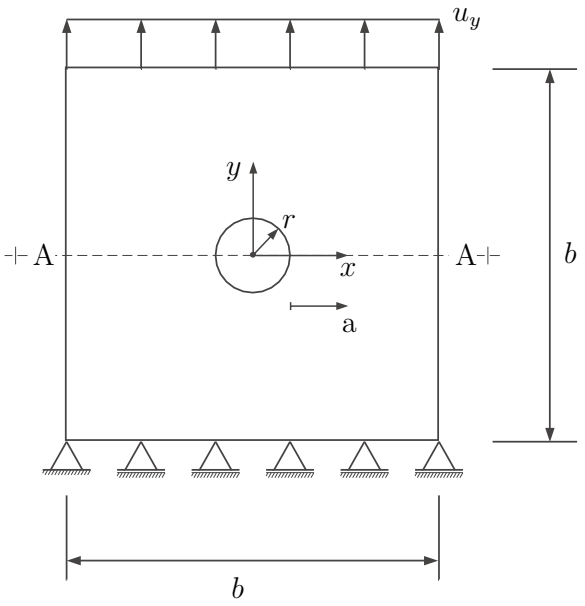

Fig. 1. Plane strain problem. The quadratic section with a circular hole is stretched in y direction.

$x \geq r$, or equivalently $a := x - r \geq 0$. For $\frac{c_7}{\mu} = 0,1mm^2$ this distribution, parameterized by $\frac{\alpha}{\mu}$, is shown in Fig. 2. It can be recognized that increasing values of $\frac{\alpha}{\mu}$ cause decreasing values of $\frac{T_{yy}}{\sigma_0}$ in the neighborhood of $a = 0$, and consequently decreasing values of stress concentration factors $\frac{T^{\star}_{yy}}{\sigma_0}$ for the micromorphic material. Note that all distributions intersect at $a = 0,13mm$.

The effect of α, c_7 on the stress concentration factor is illustrated in Fig. 3. For very large values $\frac{\alpha}{\mu}$ and values $\frac{c_7}{\mu} \geq 10^{-3}mm^2$, the stress concentration factor $\frac{T^{\star}_{yy}}{\sigma_0}$ becomes decreasing, whereas for small $\frac{\alpha}{\mu}$ the value of $\frac{T^{\star}_{yy}}{\sigma_0}$ is nearly equal to the classical one. It seems that, at fixed $\frac{\alpha}{\mu}$, $\frac{T^{\star}_{yy}}{\sigma_0}$ converges for $\frac{c_7}{\mu}$ against ∞ or 0, respectively to limits, the limit for $\frac{c_7}{\mu} \to 0$ being the classical one.

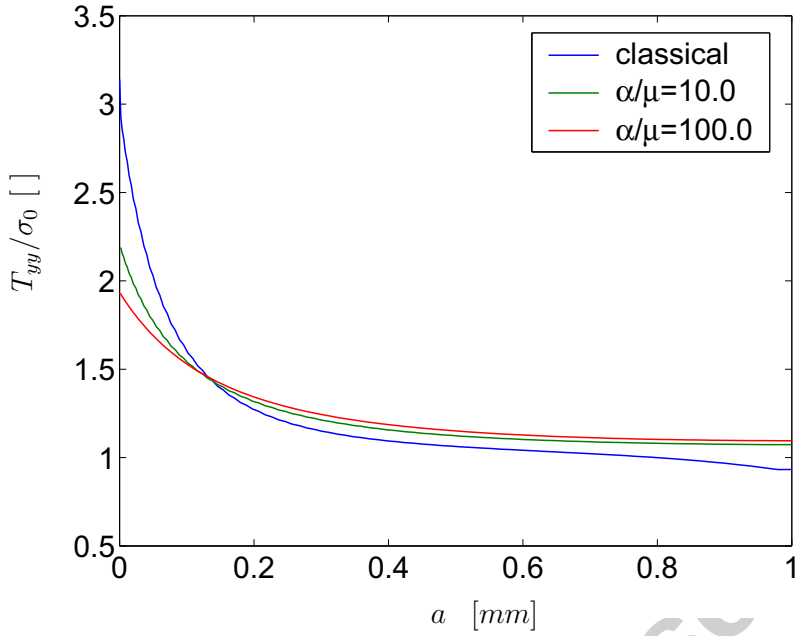

Fig. 2. Distribution of $\frac{T_{yy}}{\sigma_0}$, $T_{yy} = T_{yy}(y = 0, a \geq 0)$, for $\frac{c_7}{\mu} = 0, 1mm^2$ and varying values $\frac{\alpha}{\mu}$.

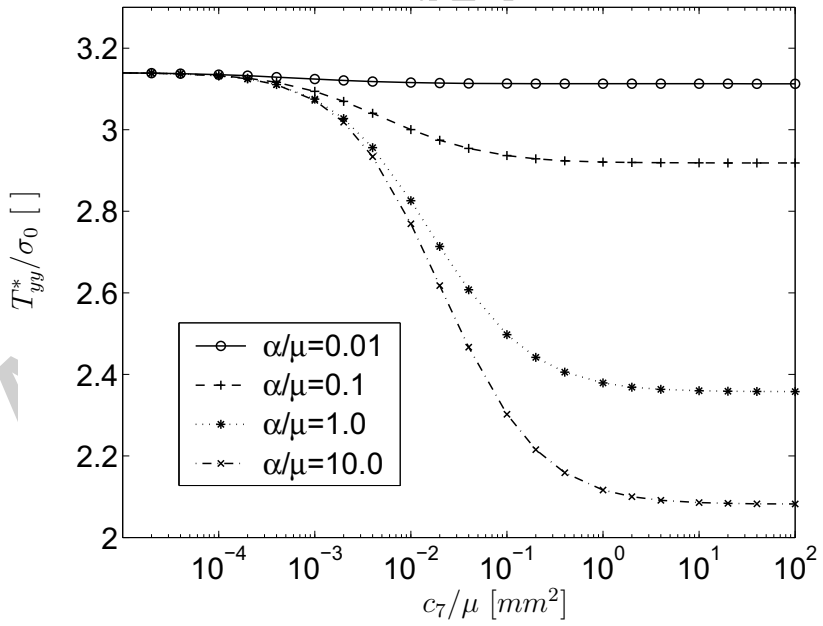

Fig. 3. Effect of α, c_7 on the stress concentration factor $\frac{T^\star_{yy}}{\sigma_0}$.

To obtain an insight into the size effects due to different, but otherwise similar boundary value problems, we ask for the stress concentration factor $\frac{T^{\star}_{yy}}{\sigma_0}$ for the cases where $\alpha \equiv \mu$ and geometry and boundary conditions of the specimens vary from each other according to a factor $n = 1, 4, 20, 200$. Corresponding results are displayed in Fig. 4, from which we deduce that all distributions are similar. In fact, if the $\frac{T^{\star}_{yy}}{\sigma_0}$ values corresponding to the specimen according to factor n are plotted as a function of $\frac{c_7}{\mu \cdot n^2}$, then all plots will coincide (see Fig. 5). In other words, for linear micromorphic elasticity, size effects may be visualized by varying the parameter c_7, the other parameters being held fixed.

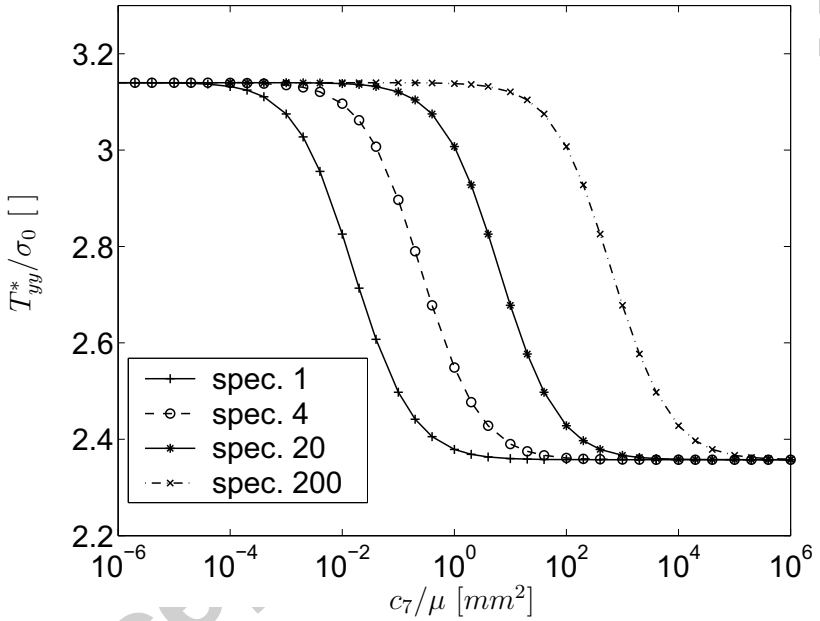

Fig. 4. Distributions of $\frac{T^{\star}_{yy}}{\sigma_0}$ against $\frac{c_7}{\mu}$, for $\alpha = \mu$ and different specimens. Geometry and boundary conditions of the specimens differ by a factor $n = 1, 4, 20, 200$, the corresponding specimens being referred to as specimen 1, ..., specimen 200, respectively.

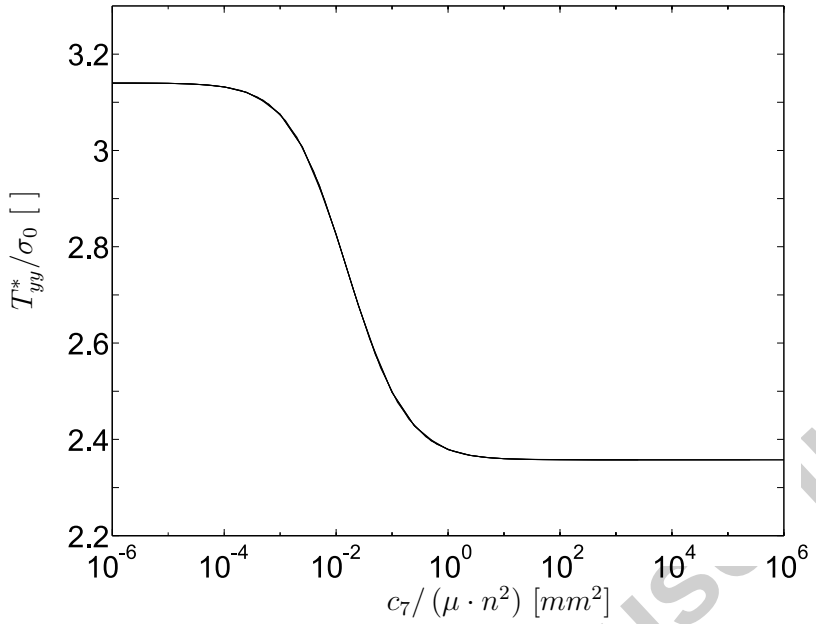

Fig. 5. Distributions of $\frac{T^{\star}_{yy}}{\sigma_0}$ against $\frac{c_7}{\mu \cdot n^2}$. The results for all specimens ($n = 1$, 4, 20, 200) are identical.

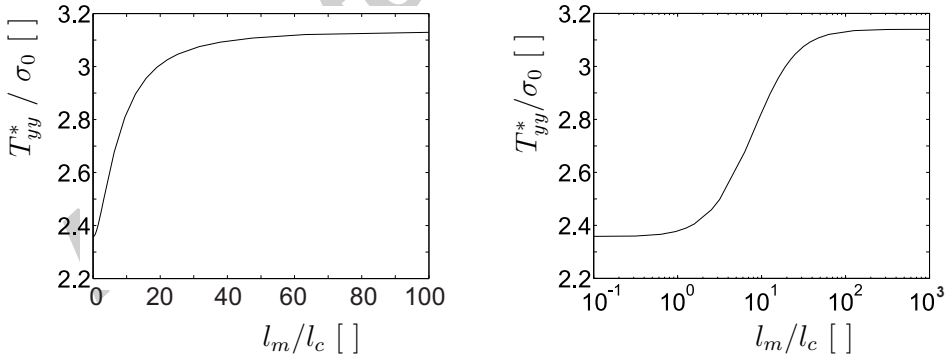

Fig. 6. Stress concentration factor $\frac{T^{\star}_{yy}}{\sigma_0}$ as a function of the ratio $\frac{l_m}{l_c}$ at $\alpha = \mu$ and $\frac{c_7}{\mu} = 0,1mm^2$; left: linear plot, right: semilogarithmic plot.

Further size effects may be elucidated by introducing a typical geometry length, as e.g. $l_m := 4r = 0,4b$. Again we concentrate ourself on specimen geometries and related boundary conditions, differing according to a factor n, with n being now $n = 0,0001,\ 0,01,\ \ldots,\ 400,\ 10000$. On choosing $\frac{c_7}{\mu} = 0,1mm^2$, the internal length l_c becomes $l_c = 0,31623mm$. It can be seen in Figure 6, that the stress concentration factor $\frac{T^{\star}_{yy}}{\sigma_0}$ is a function of the ratio $\frac{l_m}{l_c}$ (cf. also Mindlin (1963)).

2.1.2 Displacement controlled loading of cantilever rectangular beam

Further features of micromorphic elasticity may be illustrated with the aid of the cantilever rectangular beam shown in Fig. 7. We use Cartesian coordinates x, y and assume plane strain state to apply, with following boundary conditions,

$$x = 0 \quad : \quad u_y = \bar{u}_y \quad , \quad t_x = 0 \quad , \quad \mathbf{t}^{(d)} = \mathbf{0} \quad , \tag{42}$$

$$x = l \quad : \quad \mathbf{u} = \mathbf{0} \quad , \quad \mathbf{h} = 0 \quad , \tag{43}$$

$$y = 0 \quad : \quad \mathbf{t} = \mathbf{0} \quad , \quad \mathbf{t}^{(d)} = \mathbf{0} \quad , \tag{44}$$

$$y = l \quad : \quad \mathbf{t} = \mathbf{0} \quad , \quad \mathbf{t}^{(d)} = \mathbf{0} \quad , \tag{45}$$

with the given displacement $\bar{u}_y$ being uniformly distributed along the boundary $x = 0$. Again we focus attention on the effect of the material parameters α and c_7. Thereby, it is convenient to consider points, which indicate large amounts of stress gradients. Clearly, the edge point $x = l$, $y = b$ could be selected for this goal. However, such points will exhibit stress distributions with some singularities. Therefore, we shall confine the discussion on points A, B located at a distance of about $0,02 \cdot l$ and $0,17 \cdot l$, from the boundary $x = l$, respectively. Note that the length l and the height b of the beam are chosen to be $l = 3,4375mm$ and $b = 1,25mm$, while the displacement component pre-

scribed on the boundary $x = 0$ amounts $\bar{u}_y = 0,01mm$. Also, A, B are Gauss points with distances from the upper boundary $y = b$, of about $0,033 \cdot b$, respectively. However, we shall refer to such points as being located at the upper boundary $y = b = 1,25mm$. Accordingly, Fig. 8 displays the stress component T_{xx} at the boundary $y = b$, as a function of x. It may be seen, that in the neighborhood of $x = l$, the stress component T_{xx} takes vary large values, which designates the singularity in the distribution of T_{xx}.

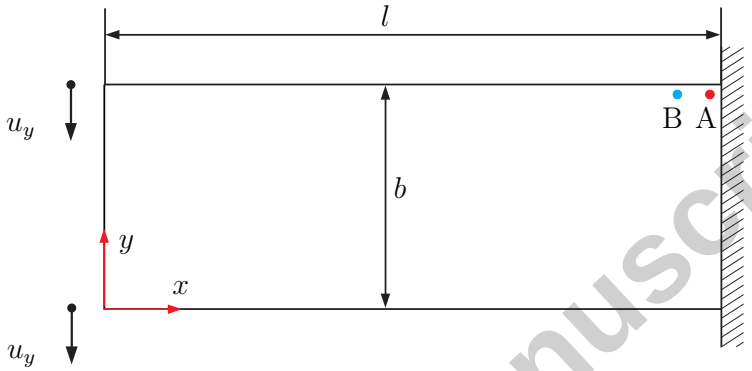

Fig. 7. Displacement controlled loading of a cantilever rectangular beam, $l = 3,4375mm$, $b = 1,25mm$, $\bar{u}_y = 0,01mm$.

Once more, we denote by "classical", solutions obtained numerically for very small values $\frac{\alpha}{\mu}$ and $\frac{c_7}{\mu}$. Fig. 9 makes clear, that in the neighborhood of the singularity (point A), stress component T_{xx} may become larger than $T_{xx}^{(class)}$, dependent on the material parameters α, c_7. However, with increasing distance from the singularity point, as e.g. at point B, T_{xx} remains smaller than $T_{xx}^{(class)}$, independent of material parameters α, c_7 (see Fig. 10).

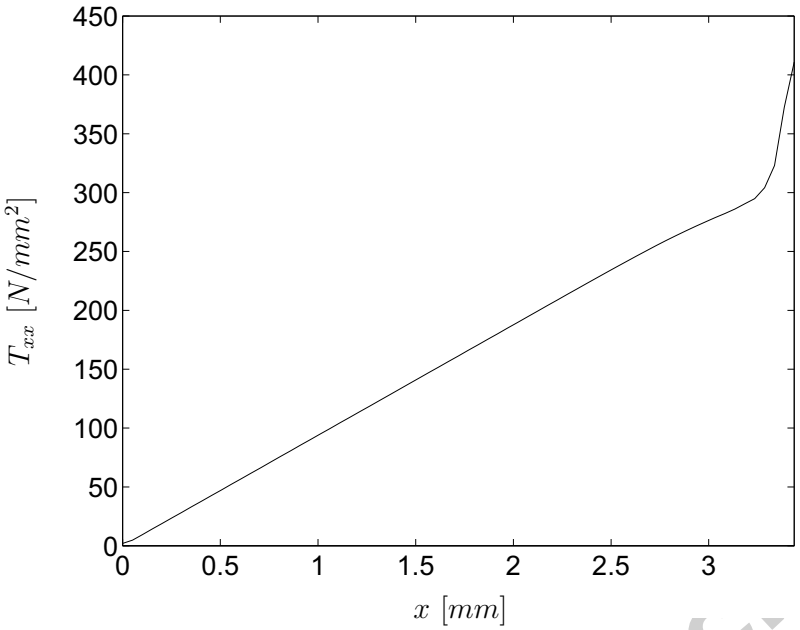

Fig. 8. Distribution of T_{xx} as a function of x, at the upper boundary $y = b = 1,25mm$, suggesting a singularity at $x = l$ ($\alpha = 10^{-8} \cdot \mu$, $\frac{c_7}{\mu} = 10^{-8}\, mm^2$).

Significant differences between the shear stress components T_{xy} and T_{yx} may be present, as can be seen in Fig. 11, for point A. Both components approach for very large values of $\frac{c_7}{\mu}$, different limits, the one for T_{xy} being vanishing. Of particular interest is also the response of the couple stress $M_c := \mathcal{T}_{xyx} - \mathcal{T}_{yxx}$, which is shown in Fig. 11 too. It can be recognized that M_c is vanishing for small values $\frac{c_7}{\mu}$, while M_c approaches a constant value for very large values $\frac{c_7}{\mu}$.

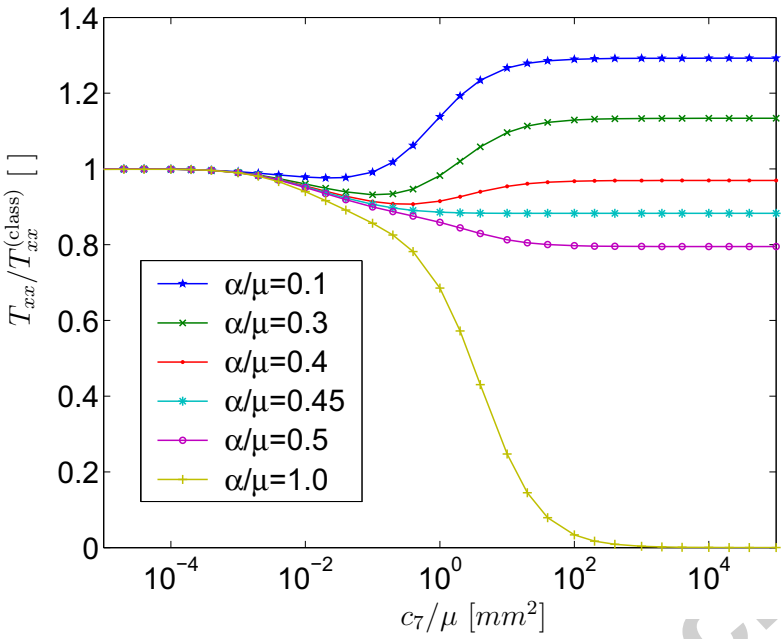

Fig. 9. Effect of material parameters α, c_7 on the response of stress component T_{xx} for point A (in the vicinity of the singular point $x = l$, $y = b$).

Finally, Fig. 12 illustrates, for fixed $\alpha = \mu$, the effect of material parameter c_7 on the deformed geometry of the beam. It may be recognized that for small values of c_7 the bending mode is dominated, while for very large values of c_7 the deformation resamples simple shear mode.

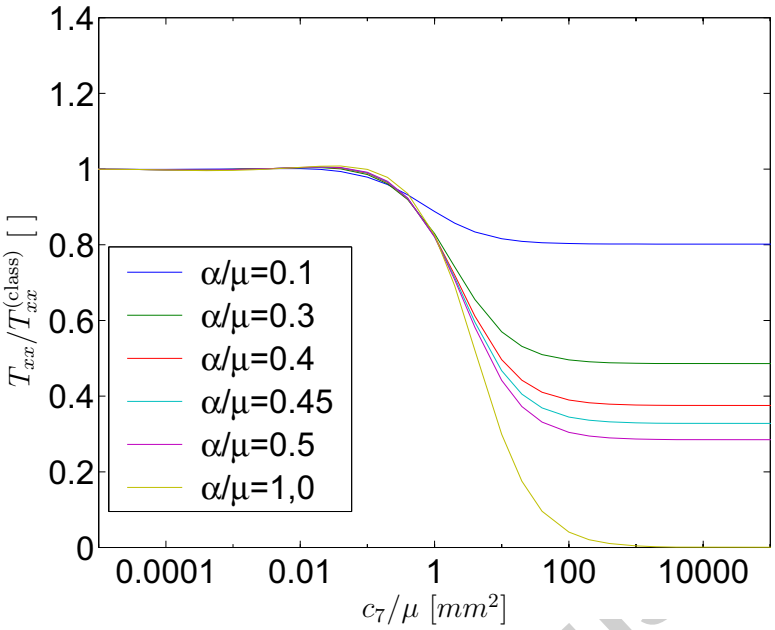

Fig. 10. Effect of material parameters α, c_7 on the response of stress component T_{xx} for point B (indicating a larger distance than point A from the singular point $x = l$, $y = b$). The values of T_{xx} are always smaller than $T_{xx}^{(class)}$.

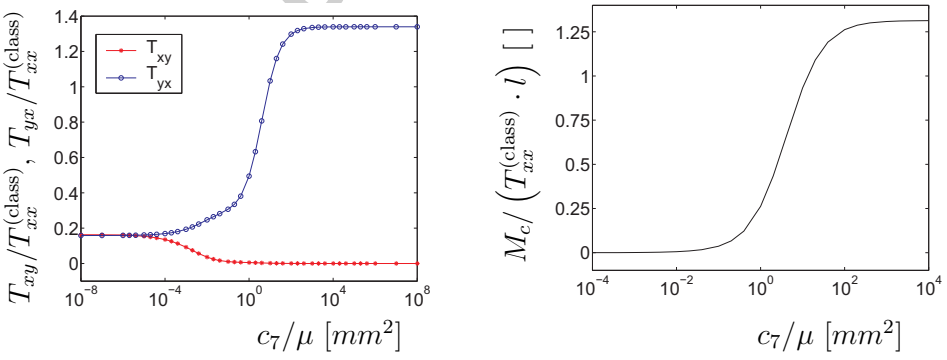

Fig. 11. Responses of T_{xy} and T_{yx} (left), as well as M_c (right), at point A ($\alpha = 1,0{\cdot}\mu$).

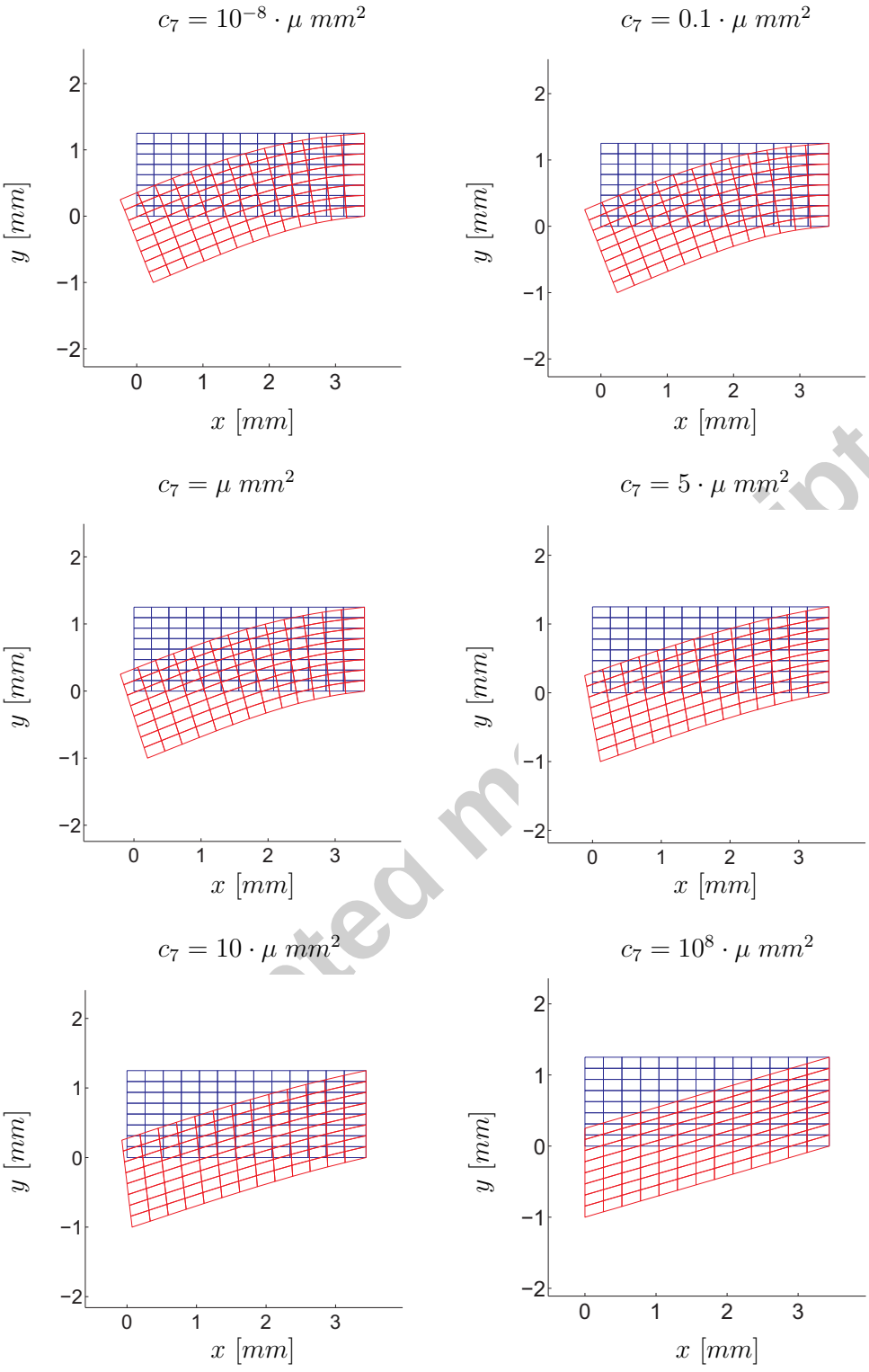

Fig. 12. Initial and deformed meshes of the rectangular beam for fixed $\alpha = \mu$ and varying material parameter c_7. Displacements u_y are presented enlarged, by factor 100. The classical case is approached for $c_7 \to 0$.

2.2 Micromorphic plasticity coupled with damage

In the following, we set

$$A_1^y \equiv 0 \quad , \quad A_2^y = 1,5 \quad , \quad A_3^y = 0 \quad , \tag{46}$$

$$B_1^y \equiv 0 \quad , \quad B_2^y = 0 \quad , \tag{47}$$

$$C_i^y \equiv 0 \quad \text{for } i \neq 7 \quad , \quad C_7^y = r_7 \neq 0 \quad , \tag{48}$$

$$k_0 = 350 N/mm^2 \tag{49}$$

in the yield function, and

$$\beta = 17 \quad , \quad \gamma = 4100 N/mm^2 \tag{50}$$

in the rule for isotropic hardening. Moreover, we fix the values of α and c_7 in the elasticity laws by

$$\alpha = 0,1 \cdot \mu \quad , \quad \frac{c_7}{\mu} = 0,1 mm^2 \quad . \tag{51}$$

2.2.1 Uniaxial loading

First, we present calculations for homogeneous uniaxial tension loading of a rectangular specimen (plane strain), according to Fig. 13. At the bottom of the specimen it is given $u_y = 0$, $t_x = 0$, $\mathbf{t}^{(d)} = \mathbf{0}$, while at the top it is $u_y = \bar{u}_y$, $t_x = 0$, $\mathbf{t}^{(d)} = \mathbf{0}$. The remaining boundaries are subject to the conditions $\mathbf{t} = \mathbf{0}$ and $\mathbf{t}^{(d)} = \mathbf{0}$. The aim is to demonstrate the capabilities of the damage model. To this end, it suffices to concentrate on isotropic hardening only. Further, as the deformations are homogeneous, no material parameters of terms related to micromorphic curvature tensors are involved. Fig. 14 shows the effect of the damage parameter α_1 (cf. Eq. (34)) on the responses of the uniaxial stress σ

and the damage variable D. Further discussion about the damage law for the classical case is provided in Lämmer and Tsakmakis (2000).

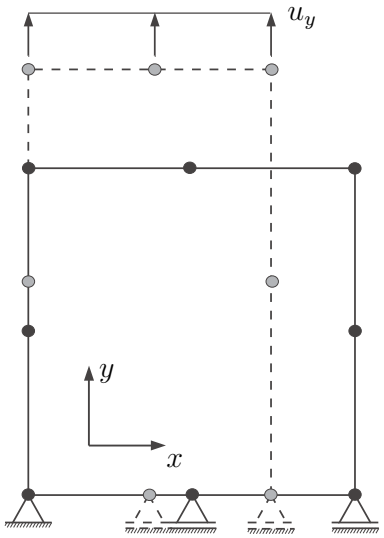

Fig. 13. Displacement controlled uniaxial loading (1 element, plain strain).

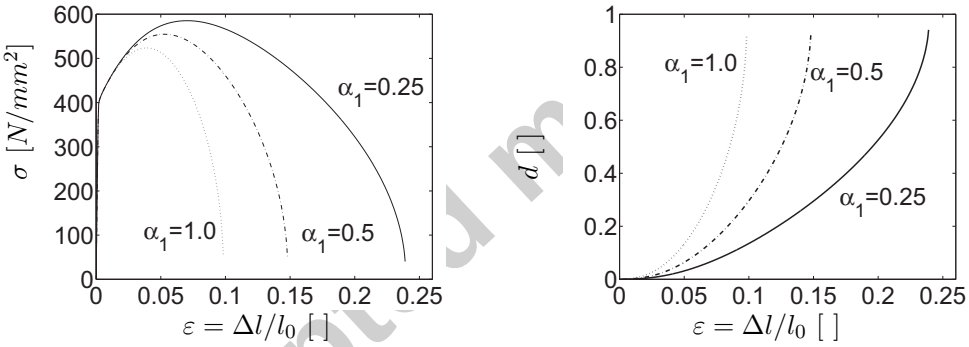

Fig. 14. Effect of material parameter α_1 on the responses of the uniaxial stress σ (left) and the damage variable D (right).

2.2.2 Rectangular specimens with circular hole under tension loading

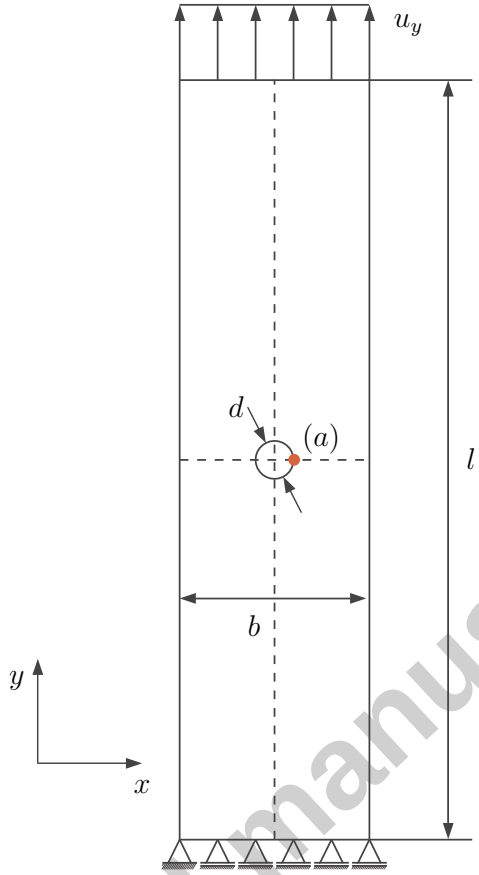

Fig. 15. Displacement controlled tension loading of rectangular sections with circular hole. All stress responses in the following figures are referred to point (a) on the hole ($x = \dfrac{b+d}{2}$, $y = \dfrac{l}{2}$).

We consider again the boundary value problem of Sect. 2.1.1, but now with respect to the specimen geometry displayed in Fig. 15 (length l differs from width b). In order to elucidate the capabilities of the micromorphic theory in predicting size effects, four specimen geometries are considered, referred to as specimens 1, 4, 20 and 200 (see Tab. 1).

First, only isotropic hardening is addressed, with material parameters as given in Sect. 2.2, and $r_7 = 10mm^{-2}$. The discussion is referred to the stress com-

ponent T_{yy} at point (a) (see Fig. 15). It can be recognized from Fig. 16 that softening for large specimens begins earlier than for small ones.

size factor n (number of specimen)	length l $[mm]$	width b $[mm]$	diameter d $[mm]$
spec. 1	10	2,5	1
spec. 4	40	10	4
spec. 20	200	50	20
spec. 200	2000	500	200

Table 1
Specimen geometries.

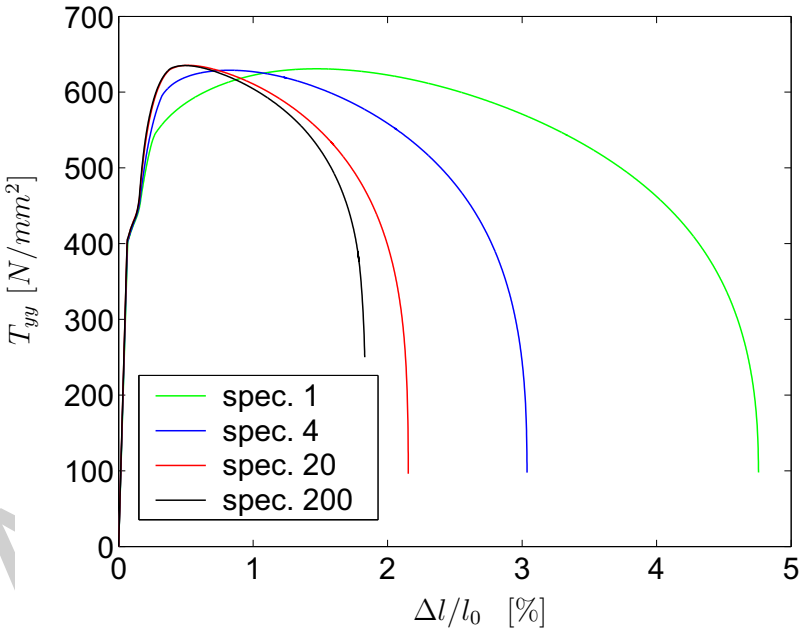

Fig. 16. Response of the stress component T_{yy} on the hole at point (a) as a function of the global strain $\dfrac{\Delta l}{l}$ ($\alpha_1 = 0.1$, $r_7 = 10mm^{-2}$).

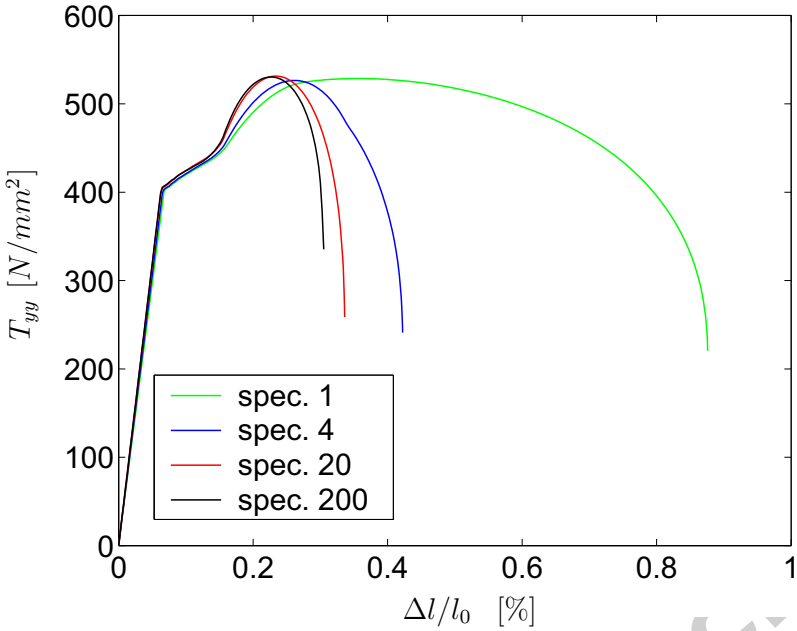

Fig. 17. Response of the stress component T_{yy} on the hole at point (a) as a function of the global strain $\frac{\Delta l}{l}$ ($\alpha_1 = 1.0$, $r_7 = 10mm^{-2}$).

Comparison of Fig. 16 ($\alpha_1 = 0, 1$) with Fig. 17 ($\alpha_1 = 1, 0$) suggests that the form of the responses is strong dependent on the damage parameter α_1. Moreover, Fig. 18 illustrates that maximal values of stresses and maximal global strains depend on the material parameter r_7, present in the yield function.

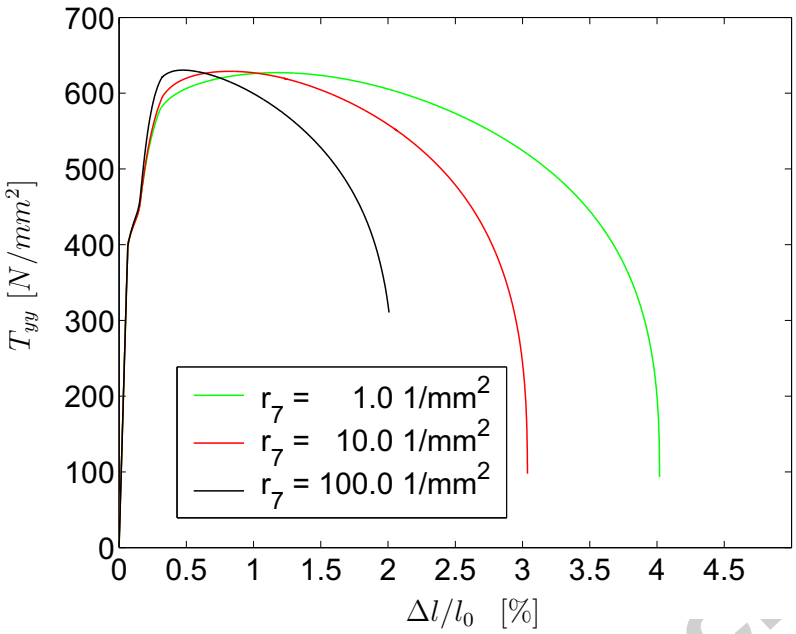

Fig. 18. Effect of the material parameter r_7 on the response of stress component T_{yy} at (a) (specimen 4, $\alpha_1 = 0, 1$).

Next, we assume the micromorphic model material to exhibit kinematic hardening only, governed by the material parameters

$$r_7 = 10mm^{-2} \quad , \quad M_2^k = 50mm^2/N \quad , \quad A_2^k = A_3^k = 200N/mm^2 \quad , \tag{52}$$

$$\mathcal{P}_7^k = 500/N \quad , \quad C_7^k = 200N/mm \quad , \tag{53}$$

the remaining material parameters related to kinematical hardening being vanishing. Similar to the case of pure isotropic hardening, Fig. 19 suggests that, softening for large specimens begins earlier than for small ones. Fig. 20 confirms that this holds also for the case of combined isotropic and kinematic hardening.

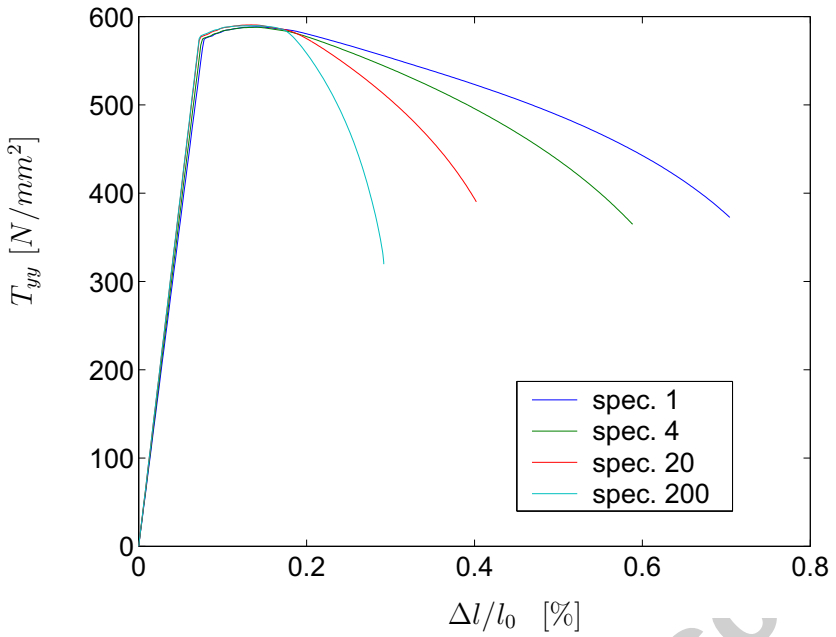

Fig. 19. Responses of T_{yy} at (a) for pure kinematic hardening ($\alpha_1 = 1$, $k_0 = 500N/mm^2$).

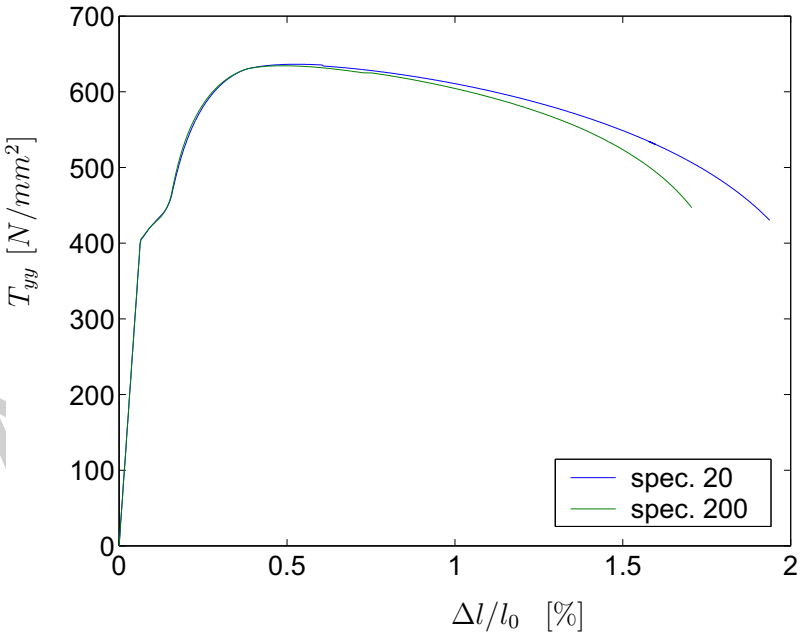

Fig. 20. Responses of T_{yy} at (a) for combined isotropic and kinematic hardening ($\alpha_1 = 1$, $k_0 = 350N/mm^2$)

3 Concluding remarks

A general framework for micromorphic plasticity has been formulated in Part I, II, incorporating isotropic and kinematic hardening. The hardening laws are of the Armstrong-Frederick type and the yield function is a generalization of the classical v. Mises yield function. Some properties of the resulting theory, concerning prediction of size effects for small deformations, are reported in Part III. However, no comparison with experimental data is available, so that it is not possible to evaluate the appropriateness of the chosen constitutive functions. This concerns over all the yield function and the isotropic hardening, the latter being unifiedly postulated. Further studies, with reference to experimental results will help to clarify such issues, but this is beyond of the scope of the present paper. All the discussions in the three articles make clear, that phenomenological micromorphic theories (at least plasticity theories) are very complicated and involve a large number of material parameters. Therefore, it will be useful to clarify in future works, if it is possible to approximate the essential material responses predicted by micromorphic theories by some simpler gradient models, which deal with classical stresses only, and involve a smaller number of material parameters. Also it is of interest to answer the following question. Is the micromorphic model appropriate enough to describe all known size effects to the necessary degree?

References

Diegele, E., Jansohn, W., Tsakmakis, C., 2000. Finite deformation plasticity and viscoplasticity laws exhibiting nonlinear hardening rules part i: Con-

stitutive theory and numerical integration. Computational Mechanics 25, 1–12.

Dillard, T., F. S., Ienny, P., 2006. Micromorphic continuum modelling of the deformation and fracture behaviour of nickel foams. European Journal of Mechanics A/Solids 25, 526—-549.

Gould, P., 1983. Introduction to linear elasticity. Springer, New York, Berlin.

Grammenoudis, P., Tsakmakis, C., 2005. Finite element implementation of large deformation micropolar plasticity exhibiting isotropic and kinematic hardening effects. International Journal for Numerical Methods in Engineering 62, 1691—-1720.

Grammenoudis, P., Tsakmakis, C., 2008. Isotropic hardening in micropolar plasticity. Archive of Applied Mechanics in press.

Hibbit, Karlsson, Sorensen, 2000a. ABAQUS theory manual, version 6.1.

Hibbit, Karlsson, Sorensen, 2000b. ABAQUS user's manual, version 6.1.

Hirschberger, C.B., K. E., Steinmann, P., 2007. On deformational and configurational mechanics of micromorphic hyperelasticity - theory and computation. Computer Methods in Applied Mechanics and Engineering 196, 4027—-4044.

Hofer, D., 2003. Simulation von größeneffekten mit mikromorphen theorien. doctoral thesis, TU Darmstadt.

Hughes, T., 1987. The Finite Element Method : Linear Static and Dynamic Finite Element Analysis. Prentice-Hall, Englewood Cliffs, New Jersey.

Kirchner, N., Steinmann, P., 2005. A unifying treatise on variational principles for gradient and micromorphic continua. Philosophical Magazine 85, 3875—-3895.

Lämmer, H., Tsakmakis, C., 2000. Discussion of coupled elastoplasticity and damage constitutive equations for small and finite deformations. Interna-

tional Journal of Plasticity 16, 495–523.

Lazar, M., Maugin, G., 2007. On microcontinuum field theories: the eshelby stress tensor and incompatibility conditions. Philosophical Magazine 87, 3853—-3870.

Mindlin, R., 1963. Influence of couple-stresses on stress concentrations. Experimental Mechanics 3, 1–7.

Neff, P., Forest, S., 2007. A geometrically exact micromorphic model for elastic metallic foams accounting for affine microstructure. modelling, existence of minimizers, identification of moduli and computational results. Journal of Elasticity 87, 239–276.

Tsakmakis, C., Willuweit, A., 2003. Time integration algorithms for finite deformation plasticity. In: Hutter, K., Baaser, H. (Eds.), Deformation and Failure of Metallic Continua. Springer, pp. 79–106.

Tsakmakis, C., Willuweit, A., 2004. A comparative study of kinematic hardening rules at finite deformations. International Journal of Non-Linear Mechanics 39, 539—554.

Weber, G., Anand, L., 1991. Finite deformation constitutive equations and a time integration procedure for isotropic, hyperelastic-viscoplastic solids. Comp. Meth. Appl. Mech. Eng. 79, 173–202.

Weber, G., Lush, A., Zavaliangos, A., Anand, L., 1990. An objective time-integration procedure for isotropic rate-independent and rate-dependent elastic-plastic constitutive equations. Int. J. Plasticity 6, 701–744.